

Article

Porous Titanium for Biomedical Applications: Evaluation of the Conventional Powder Metallurgy Frontier and Space-Holder Technique

Sheila Lascano ^{1,*} , Cristina Arévalo ² , Isabel Montealegre-Melendez ² , Sergio Muñoz ²,
José A. Rodríguez-Ortiz ², Paloma Trueba ² and Yadir Torres ^{2,*}

¹ Departamento de Ingeniería Mecánica, Universidad Técnica Federico Santa María, Avda. Vicuña Mackenna Poniente N° 3939- San Joaquín, 8320000 Santiago, Chile

² Departamento de Ingeniería y Ciencia de los Materiales y del Transporte, E.T.S. de Ingeniería-Escuela Politécnica Superior, Universidad de Sevilla, Camino de los Descubrimientos, s/n. 41092 Sevilla, Spain; carevalo@us.es (C.A.); imontealegre@us.es (I.M.-M.); sergiomunoz@us.es (S.M.); jarortiz@us.es (J.A.R.-O.); ptrueba@us.es (P.T.)

* Correspondence: sheila.lascano@usm.cl (S.L.); ytorres@us.es (Y.T.); Tel.: +56-2-23037262 (S.L.)

Received: 1 February 2019; Accepted: 4 March 2019; Published: 8 March 2019



Abstract: Titanium and its alloys are reference materials in biomedical applications because of their desirable properties. However, one of the most important concerns in long-term prostheses is bone resorption as a result of the stress-shielding phenomena. Development of porous titanium for implants with a low Young's modulus has accomplished increasing scientific and technological attention. The aim of this study is to evaluate the viability, industrial implementation and potential technology transfer of different powder-metallurgy techniques to obtain porous titanium with stiffness values similar to that exhibited by cortical bone. Porous samples of commercial pure titanium grade-4 were obtained by following both conventional powder metallurgy (PM) and space-holder technique. The conventional PM frontier (Loose-Sintering) was evaluated. Additionally, the technical feasibility of two different space holders (NH_4HCO_3 and NaCl) was investigated. The microstructural and mechanical properties were assessed. Furthermore, the mechanical properties of titanium porous structures with porosities of 40% were studied by Finite Element Method (FEM) and compared with the experimental results. Some important findings are: (i) the optimal parameters for processing routes used to obtain low Young's modulus values, retaining suitable mechanical strength; (ii) better mechanical response was obtained by using NH_4HCO_3 as space holder; and (iii) Ti matrix hardening when the interconnected porosity was 36–45% of total porosity. Finally, the advantages and limitations of the PM techniques employed, towards an industrial implementation, were discussed.

Keywords: biomaterials; titanium; powder metallurgy; loose sintering; finite element method; mechanical behaviour

1. Introduction

Nowadays, most of the research efforts are focused on the development of metallic biomaterials for bone replacement. Among all biomaterials, it is widely known that titanium and its alloys are the candidates with the best in vitro and in vivo behaviour. However, the stress-shielding phenomenon remains a concern in their use for biomedical applications. The stress shielding is associated with the mismatch between the Young's modulus of bone tissue and titanium (cortical bone around 20–25 GPa and titanium 110 GPa) [1], which causes bone resorption and eventual fracture of the host cortical bone surrounding the implants [2,3].

The design and manufacturing of implants with lower stiffness materials could be a solution for this problem [4] and several works conducted aiming to develop scaffolds with a suitable balance between mechanical and biofunctional behaviour [5–7]. Currently, there are different methods to reduce the stress shielding, such as: (i) Polymer matrix compounds. An example of this kind of biomaterial is the HAPEX[®], composed by 40% hydroxyapatite and 60% HDPE (High Density Polyethylene), although it is not used for load-bearing applications due to their limited mechanical properties [8]. (ii) Metastable β -titanium alloys. These materials have lower moduli (55–90 GPa) and have been in development since the 1990s. Even the low moduli monolithic Ti alloys are significantly stiffer than bone [9]. Their medical use is also conditioned for their low wear resistance and limited strength. Important advances in new Ti-Nb-Ta-Mn alloys represent a promising way to solve problems related to stress shielding but still the reduced strength of the samples is considered a concern [10]. (iii) Porous materials. Up to 34 processing routes to fabricate porous materials have been reported [11–13]. The objective of many of these methods is the manufacturing of titanium foams [14–20], in which the porosity percentage must be controlled with the aim to reduce the implant stiffness without any undesirable influence on the mechanical properties [21]. In this context, the limitations in controlling the quantity, size, distribution and morphology of the pores by conventional routes should be considered. Furthermore, the high cost, and the great difficulty in obtaining reproducibility and versatility of the new processing routes (laser sintering, ion beam milling, field-assisted sintering technology (FAST), etc.) should be also contemplated. On the contrary, both the powder-metallurgy processing and the space-holder technique provide a suitable route to obtain Ti porous structures [21]; they also have a remarkable advantage because they are an economical and non-toxic methods, without a toxic agent that can affect cellular functions.

From a powder-technology point of view, porous titanium could be produced by several methods [12,13,17–25]. The performance of porous titanium via conventional Powder Metallurgy (PM) offers flexibility and it is also a cost-effective alternative. Among the different techniques, there are interesting manufacturing processes where low compaction pressures are employed because of higher porosities and a lower Young's modulus can be obtained. Loose sintering (LS) is an attractive method to produce porous specimens. In this process, compaction pressure is not applied. In this way, specimens produced by this technique have higher porosity than specimens fabricated via conventional PM. Despite that, there are not so many works where the porous titanium could be produced at low compaction pressure [1]. In order to solve the limitations of conventional PM, space holder techniques help to control porosity parameters such as pore morphology and percentage [1,15,26–31].

In addition, the effective material response can be determined experimentally or numerically. Although the experimental characterization cannot be replaced entirely by numerical methods, numerical analyses complementing the experimental characterization may serve to reduce the experimental effort significantly, filling gaps in experimentation. In this sense, numerical models have the potential to provide a deeper insight into the underlying microstructural mechanisms of deformation and thus a deeper understanding of the material behaviour. Finite Element Method (FEM) is presented as a useful technique to generate the models of titanium foams in order to obtain mechanical properties [32].

Therefore, within the above context, the aim of the present study is to appraise the feasibility and repeatability of described processing techniques: conventional PM, LS and space-holder technique. In addition, the mechanical properties of porous structures have been assessed by FEM. The results obtained are compared in order to evaluate those different techniques, in terms of advantages and limitations, and the particular features of each fabrication route. The present work has been concluded with a summary of the most favourable technique according to industrial viability, economic benefits and reproducibility, achieving an optimal equilibrium between mechanical properties and biofunctional behaviour.

2. Materials and Methods

Commercially pure titanium (cp Ti) powder produced by a hydrogenation/dehydrogenation process has been used as the starting powder (SE-JONG Materials Co. Ltd., Incheon, Korea). Its chemical composition is equivalent to cp Ti ASTM F67-00 Grade IV. Two different space holders have been employed: sodium chloride, NaCl (Panreac Química S.A.U., Barcelona, Spain, purity > 99.5%) and ammonium bicarbonate, NH_4HCO_3 , (Cymit Química S.L, Barcelona, Spain, with a purity of 99.9%). The space-holder granules, NaCl and NH_4HCO_3 , with a large particle size (according to Table 1) were selected to promote a higher degree of interconnectivity of the pores, and a high average size of space holder (>100 μm) would fulfil the requirements to ensure the bone ingrowth.

Table 1. Particle size distribution of materials used.

	$d_{[10]}$, μm	$d_{[50]}$, μm	$d_{[90]}$, μm
Ti powder	9.7	23.3	48.4
NaCl	183.0	384.0	701.0
NH_4HCO_3	73.0	233.0	497.0

In order to obtain the green bodies, conventional PM at low pressure (including its particular limits: loose sintering, LS) and space-holder techniques have been implemented. In an LS route, the metal powder has been poured and vibrated into a cylindrical mould of alumina for 2 min, which has then been heated to the sintering temperature chosen (1000 °C and 1200 °C) under high vacuum ($\sim 10^{-5}$ mbar). In the space-holder technique: (1) the blends of cp Ti powder and space-holder particles [cp Ti+NaCl or cp Ti + NH_4HCO_3], only powder mixtures with 30 and 40 volume percent of space holders were prepared in a Turbula[®] T2C, blended for 40 min to ensure good homogenization; (2) afterwards, the compaction of the mixture takes place (800 MPa, pressure defined according to the compressibility curve of the material and the results of a previous work [26]), (3) subsequently, regarding to the space holder used, the elimination step has been performed. The NH_4HCO_3 is thermally removed (60 °C + 110 °C; both stages of the thermal treatment are carried out for 10–12 h and at low vacuum conditions 10^{-2} mbar) [26], while the salt has dissolved in distilled water (temperature between 50 and 60 °C, without agitation and during 4–5 immersion cycles) [19]. Sintering was carried out under high vacuum in a CARBOLYTE STF 15/75/450 ceramic furnace with a horizontal tube (2 h at 1250 °C under high vacuum conditions: $\sim 10^{-5}$ mbar) [26].

The manufacturing parameters have been established in order to obtain mechanical properties (Young's modulus, E , and yield strength, σ_y) similar to the cortical bone. The powder mass has been calculated to produce specimens with fit dimensions for compression tests (height/diameter = 0.8). The compaction stage in conventional PM and space-holder technique has been carried out in an INSTRON 5505 machine (Instron, Massachusetts, United State).

Density measurement has been performed out through the Archimedes' method with distilled water impregnation, due to its experimental simplicity and reasonable reliability (ASTM C373-88). Total porosity $P(\text{Arch})$ and interconnected porosity (P_i) have been calculated from the density measurements. For the image analysis, sectioned parts have been prepared by a sequence of conventional metallographic steps (resin mounting and grinding) followed by a mechanic-chemical polishing with magnesium oxide and hydrogen peroxide. The porosity evaluation by image analysis has been performed by using an optical microscope Nikon Epiphot (Nikon, Tokyo, Japan) coupled with a camera Jenoptik Progres C3 (Jenoptik, Jena, Germany), and the software Image-Pro Plus 6.2, Mediacibernetica, Bethesda, MD, USA. Image analysis has been evaluated with 10 pictures of 5 \times and 20 \times for each processing condition. The following morphological pore parameters have been estimated by this method: (i) the total porosity $P(\text{IA})$, (ii) equivalent diameter (D_{eq}) defined as the average diameter measured from the pore centroid, (iii) the pore shape factor, $F_f = 4\pi A / (PE)^2$, where A is the pore area and PE is the experimental perimeter of the pore, (iv) the mean free path between the pores is

described as the mean size of the necks between the pores, λ , and (v) the pore interconnectivity (C_{pore}) is defined as the fraction of connected pores of the total reference line length. Light Microscopy (LM) has also been used for the basic observation of the microstructural features of the surface samples.

The mechanical compression testing has been achieved according to the recommendations of the Standard ASTM E9-89A, by means of a universal electromechanical Instron machine 5505 applying a strain rate of 0.005 mm/mm·min. All tests have been run up to a strain of 50%. The yield strength (σ_y), relative strength (defined as the ratio between the strength of porous material and the bulk material) and Young's modulus (E_c) have also been determined. Furthermore, dynamic Young's modulus (E_d) measurements by the ultrasound technique have been performed [26,33]. Three specimens have been tested in order to calculate a mean value of dynamic Young's modulus. Previously, the specimens have been characterised by porosity measurements (density) and mechanical compression testing.

Finally, FEM was implemented to conduct the numerical characterization of mechanical properties (Young's modulus, E , and yield strength, σ_y) for the sample with 40 vol.% of porosity developed in this work. For this, a 2D finite element model proposed by the authors [6,34] was used. This numerical model, based on geometries generated from information of the pore morphology, combines a 2D periodic geometry with the information of the pore morphology extracted from image analysis ($P(IA)$, pore size distribution, and elongation factor, F_e).

3. Results

This section may be divided by subheadings. It should provide a concise and precise description of the experimental results, and their interpretation as well as the experimental conclusions that can be drawn.

3.1. Physical and Microstructural Properties

LM micrographs and parameters associated to porosity ($P(IA)$, D_{eq} , F_f , λ and C_{pore}) are shown in Figure 1 and Table 2. These parameters are related to the researched processing routes: conventional PM technique (compaction pressure (0 and 13 MPa) and sintering temperature (1000 and 1200 °C)) and space-holder technique (type (NaCl and NH_4HCO_3) and space-holder content (30 and 40 vol.%)). For the last route, compaction pressure and sintering temperature have been fixed in 600 MPa and 1250 °C, respectively.

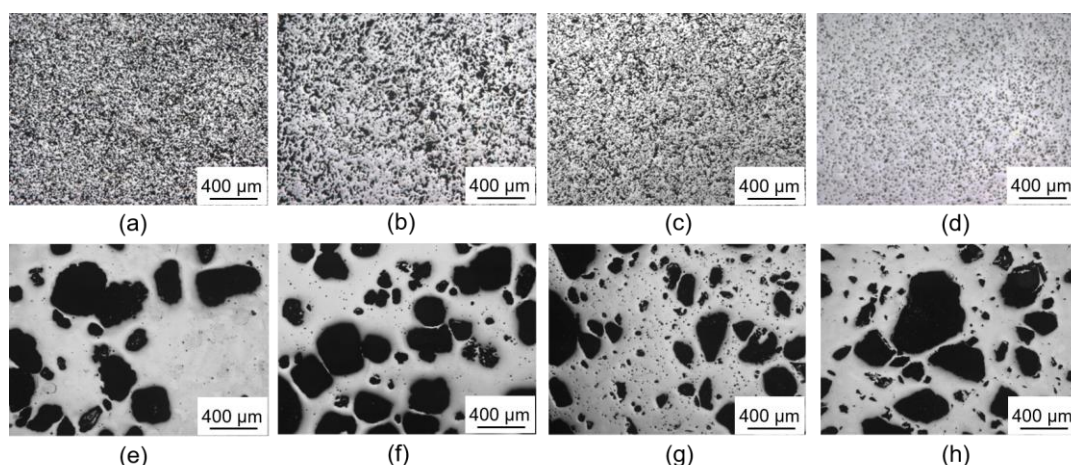


Figure 1. Micrographs corresponding to different processing conditions of evaluated techniques: Loose Sintering, conventional Powder Metallurgy (PM) and space-holder technique: (a) 0 MPa and 1000 °C; (b) 0 MPa and 1200 °C; (c) 13 MPa and 1000 °C; (d) 13 MPa and 1200 °C; (e) 30 vol.% NaCl; (f) 40 vol.% NaCl (g) 30 vol.% NH_4HCO_3 ; and (h) 40 vol.% NH_4HCO_3 . All of the samples have been sintered for 2 h under high vacuum ($\sim 10^{-5}$ bar).

Table 2. Effect of different techniques and processing conditions on the porosity of the samples.

Processing Conditions		Archimedes			Image Analysis			
		P_i , %	$P(\text{Arch})$, %	$P(\text{IA})$, %	D_{eq} , μm	F_f	C_{pore}	λ , μm
Loose Sintering	1000 °C	44.1	44.8	45.3	17	0.70	0.2	25
	1200 °C	28.5	35.2	30.0	15	0.82	0.1	41
13 MPa	1000 °C	28.0	29.3	30.8	14	0.79	0.1	36
	1200 °C	6.2	13.6	13.1	10	0.93	0.0	66
Space holder	30 vol.% NaCl	20.5	28.5	28.4	47.0	0.90	0.3	157
	40 vol.% NaCl	27.5	35.8	35.1	78.0	0.74	0.2	181
	30 vol.% NH_4HCO_3	22.4	27.8	29.1	18.1	0.90	0.3	57
	40 vol.% NH_4HCO_3	29.3	37.6	36.6	32.0	0.84	0.3	80

3.2. Mechanical Properties

In this work, the influence of the manufacturing technique that would lead to obtaining an optimal equilibrium between the mechanical strength and the Young’s modulus in order to replace the cortical bone (150–200 MPa and 20–25 GPa, respectively) is analysed. Table 3 summarizes the results of mechanical compression testing and ultrasound technique.

Table 3. Effect of different techniques and processing conditions on mechanical properties of the samples obtained by compression test and ultrasound testing.

Processing Conditions		Experimental		
		σ_y , MPa	E_c , GPa	E_d , GPa
Loose Sintering	1000 °C	67	9.6	29.1
	1200 °C	165	25.1	50.5
13 MPa	1000 °C	200	12.5	50.1
	1200 °C	350	26.1	59.4
Space holder	30 vol.% NaCl	415	4.6	45.1
	40 vol.% NaCl	187	5.3	29.0
	30 vol.% NH_4HCO_3	389	15.9	38.9
	40 vol.% NH_4HCO_3	272	5.8	30.0

In addition, the influence of the total porosity in the Young modulus (by ultrasound technique) is illustrated in Figure 2. As expected, the material stiffness presents a direct relation to the effective area of the titanium matrix (inverse to the porosity). Mathematical models are also added to fit the experimental results: Gibson and Ashby [35], Pabst-Gregorová [36], and Knudsen [37] and Spriggs [38].

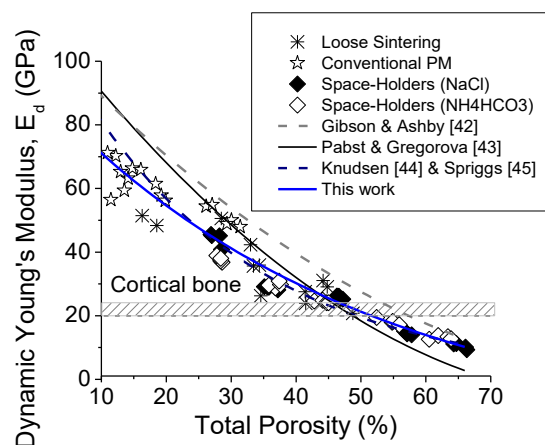


Figure 2. Dynamic Young modulus vs. total porosity: Influence of the manufacturing route.

In the present work, a new and suitable model is proposed in order to represent the experimental results in porous titanium materials from total porosity between 10 and 60 vol.% (see in Equation (1)):

$$E = E_{Ti} \left(e^{-0.02P} \right) - 0.03E_{Ti}, \tag{1}$$

where E_{Ti} is the Young’s modulus for bulk titanium and P is the total porosity of the sample.

Moreover, in previous research, different models have been developed to explain the correlation between the relative strength and the density in sintered materials. In the geometric model, spherical pores are assumed [39]. It is based on the geometrical relation between the porosity and the cross section area of the material. In addition, there is a model known as “simple Brick” where the pores with a cubic geometry are supposed [40]. The relative strength is determined in this method, considering the probability of being found a solid part in the tested volume. A correlation between the relative strength vs. density and interconnected porosity of the porous titanium specimens, produced via conventional PM and space-holder techniques, are shown in Figure 3a,b, respectively.

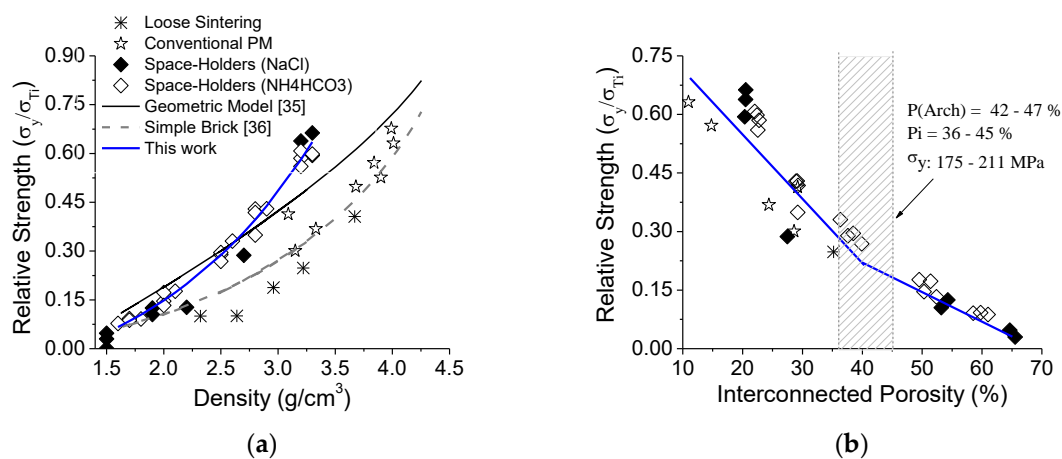


Figure 3. (a) Density vs. Relative Strength; (b) Interconnected Porosity and Relative Porosity vs. Relative Strength (porous material strength/full dense material strength).

The analysis of mechanical behaviour of specimens produced via conventional PM, could be estimated using the simple brick model; however, the geometrical model is not capable of predicting any tendency. Therefore, in Equation (2), an exponential model is proposed in order to fit successfully the type and range of pores, which are produced by the space -holder technique:

$$\frac{\sigma_y}{\sigma_{Ti}} = \left(1.88 e^{-3P} \right) - 0.2. \tag{2}$$

3.3. Finite Element Simulation

The case under study chosen in this numerical analysis is the porous compact fabricated following the space holder technique, by using ammonium bicarbonate, NH_4HCO_3 , as a space holder and obtaining a 40 vol.% of total porosity. This is the porous compact that has shown the most interesting mechanical properties, with the best balance between stiffness and mechanical integrity and, consequently, the ideal candidate for the use in cortical bone replacement. Following the methodology described by Muñoz et al. [6,34], and making use of the main porosity characteristics extracted from experiments (total porosity, pore size distribution and elongation factor distribution), one finite element geometry has been randomly generated for the porous materials under study: 40 vol.% of total porosity. The simulated microstructure of the porous material is comprised of two different phases: a titanium matrix and a series of pores randomly distributed. The mechanical properties of cp Ti have been used to describe the behaviour of the titanium matrix: a Young’s modulus $E_{Ti} = 110$ GPa, a yield stress

$\sigma_{Ti} = 700$ MPa and a Poisson's ratio $\nu = 0.33$. In order to describe the hardening plasticity behaviour of titanium, an isotropic hardening with a very small tangent modulus $E_T = 1$ GPa has been used. The pore morphology (equivalent diameter, D_{eq} , and elongation factor, F_e) has randomly generated following a normal distribution from the experimental data. The following values have been extracted from experimentation to be used in the pore generation: $D_{eq} = 32$ μm and $F_e = 0.65$. In addition, the pore orientation has also been randomly generated following a uniform distribution.

Making use of the FE models, two different compression tests have been simulated. First, with the aim of predicting the mechanical properties of the porous material, a compression test under displacement control up to 1% macroscopic strain has been simulated. Then, the predicted uniaxial stress–strain responses have been obtained. The results in the simulation are summarized in Table 4.

Table 4. Prediction of mechanical properties for the case of study corresponding to a porous compact fabricated by 40 vol.% NH_4HCO_3 space holder.

Properties	Experimental	FEM
E , GPa	31	39
σ_y , MPa	170	153

From the presented results, it can be seen that very good agreement is achieved with the proposed FE model, for both Young's modulus and yield stress.

Second, in order to complete the numerical analysis and for a better understanding of the mechanical behaviour of the porous material, the stress distribution within the porous matrix has been analysed in detail. By using the proposed FE model, a compression test under displacement control was performed until the macroscopic yield is reached ($\sigma_y = 170$ MPa, in this case). The results of this virtual test can be seen in Figure 4, where the contour plot of the von Mises stress distribution at macroscopic yield is shown.

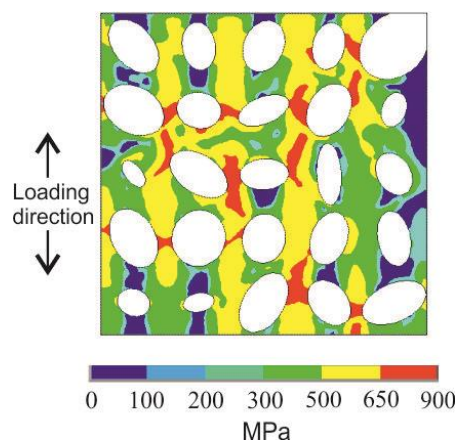


Figure 4. Example of Von Mises stress distribution at macroscopic yield. The case studied corresponding to a porous compact fabricated by a 40 vol.% NH_4HCO_3 space holder.

In Figure 4, it can be observed that, even though the applied macroscopic stress is only 170 MPa, there is a considerable portion of the material with a high stress level, due to stress concentration around the pores, as it could be expected.

4. Discussion

In the present study, potentialities and disadvantages of different processing routes are compared in terms of: viability (cost and potential industrial application), reproducibility (reliability), limitations (porosity range, size, shape and distribution) and transversality of established or optimized protocols

to other interested emerged and/or higher value added sectors. The framework used to make that comparison is based on the capability to achieve an optimum equilibrium between mechanical (E and σ_y , according according to bone tissue to substitute) and biofunctional behaviour (allowing bone ingrowth and obtaining an inside porous roughness to improve osteointegration and infiltration with bioactive materials).

Concerning to the microstructural results, in conventional PM, compaction pressure and sintering temperature have a significant effect in porosity (see Table 2). In general, temperature has the highest effect over porous morphological parameters as well as final porosity. For the temperature range studied, when temperature increases, an approximately 70% porosity reduction is observed. Porosity range that can be achieved through the implementation of this technique is from 13.6% to 44.8%, reaching the highest values by LS at 1000 °C sintering temperature. In this case, the porosity becomes more interconnected (44.1% at 0 MPa and 28.0% at 13 MPa). As it was expected, when temperature increases: (a) pore size is reduced, a 12% for 0 MPa compaction pressure level and a 29% for the highest pressure value; (b) pores are more rounded (shape factor, F_f , close to one); (c) closed or isolated porosity is higher; (d) porous contiguity decreases until reaching zero value (isolated porosity); and (e) the distance between porous is 2.64 higher. Moreover, in general, compaction pressure effect is lower than the temperature influence.

Regarding to the space-holder technique, the type of space holder used defines the porous morphology (irregular surface), fracture behaviour and plastic deformation of the specimens. These factors could affect, to some extent: (1) preserving the pore size (related to the space-holder volume); (2) the pore walls roughness; (3) increasing of interconnectivity between the pores; (4) the collapse of the porous structure of specimens (structural integrity of the samples during the process of space-holder evacuation); (5) the manufacturing cost of the specimens (time and resources); (6) the reproducibility of the evacuation space-holder process (it depends on the number and control of the process parameters) and (7) the risk of the residual space-holder content, from the point of biomedical view.

In this context, considering the range of compaction pressure, it is observed how the use of space holders allows for achieving higher porosity levels and similar sizes to the original space holder distribution compared to the conventional PM technique.

The total porosity could be controlled by varying space-holder content, although a small proportion of isolated micro-porosity has been observed (Figure 1 and Table 2). This micro-porosity is produced during the sintering of titanium powders.

The role and the comparison of the studied space-holder size (NaCl and NH_4HCO_3) should be analysed by considering the particle size distribution of the starting powders (Table 1). By using 30 vol.% of space-holder content, D_{eq} of the obtained pores is around 2.6 greater employing NaCl. Although the differences between the obtained D_{eq} can lead to a decrease in a 15% using 40 vol.% of space holder. The increasing of interconnectivity (λ) for NH_4HCO_3 implies balances between the differences due to an original space-holder size employed.

Moreover, a round shaped porosity is formed (slightly shape boundary related to the sintering stage). Nevertheless, a small part of the porous, for NaCl as a space-holder, could be preserving the cubic geometry according to the original morphology, whereas the pores are shaped due to the employment of the NH_4HCO_3 showing an elliptical and elongated morphology. Additionally, the porous titanium specimens produced by NH_4HCO_3 manifest a better porous homogeneity distribution than the ones fabricated with NaCl; during the powder compaction, the NaCl is less fractured than the NH_4HCO_3 . In spite of that, the NaCl removal is more costly, less repeatable and less feasible to industrial implementation.

Regardless of the nature of the space-holder, increasing their content has some important outcomes: pore shape factor is reduced (irregular morphology of porous boundary); the contiguity (C_{pore}) is kept constant for both cases; interconnected porosity for 30 vol.% of space holder represents the 75% of the total porosity, while 40 vol.% of space holder reaches 78 %. Both values of the interconnected

porosity and the suitable size of the pores promote the bone ingrowth. However, its influences on the mechanical behaviour should be considered (see below).

At this point of this reported research, the results and discussion have been focused on the analysis of each fabrication method independently, where the influence of the processing parameters on the porosity has been evaluated. The following stage is now emphasised on a general comparison of both processing routes. A significant difference in morphology and porosity distribution among the specimens produced via conventional PM and a space-holder technique is observed (see in Figure 1). In conventional PM, the obtained pores present an irregular shape and a more homogenous distribution than in the space-holder process, in which the morphology of the pores reproduces the employed space-holder geometry. The D_{eq} obtained by using a space holder are larger than those resulted from the conventional PM (Table 2). These results verify the potential and versatility of the space-holder method to control the shape, the size, the proportion and distribution of the porosity, in order to achieve biofunctional and biomechanical equilibrium of the implants. This notwithstanding, both industrial application viability and low cost of conventional PM routes are well known features.

Within the context of porous implants in contact with bone tissue, some previous papers have reported that a suitable bone ingrowth can be achieved with a mean pore size of around 50 μm [41,42]. However, there are other studies where the optimal bone ingrowth happens for pore size range of 100–200 μm [9,43,44]. Nevertheless, several authors' works show a better infiltration achievement with polymers or bioactive glasses if the pore size overcomes 200 μm [45]. Accordingly, the conventional PM route manifests a drawback and thus only 6% of the pores (0 MPa and 1000 °C), which assures doubtful bone ingrowth, being almost a non-existent possibility to perform infiltration tests. On the other hand, the space-holder method allows for achieving successful results of optimal bone growth and better infiltration of the polymers or bio-glasses in the pores [45].

Considering the mechanical behaviour analysis results (Figure 2), to achieve a suitable stiffness range (20–25 GPa), it is necessary to obtain a total porosity between 40–55%. It could be achieved by using conventional PM, only when temperature and pressure are in the limits of this technique (0 MPa and sintering temperatures 1000 °C and 1100 °C), although there is a notable loss of the mechanical strength (see below). However, the space-holder technique presents a great feasibility to get these values of total porosity and even to lower stiffness values (6–8 GPa at higher porosity), it being possible to replace the trabecular tissue by these obtained results.

Concerning mechanical properties, two different analyses have been made, aiming at the evaluation of the role of the manufacturing route tested in the compression behaviour (Figure 5). Independent of the processing technique used, a parameter is fixed for each comparison: in Figure 5a, Young's modulus close to the cortical bone is set in ~29 GPa (porosity total range between 37.6–44.8%) and the influence of the processing technique on the yield strength (σ_y) of the porous specimens is studied. In order to reach the same Young's modulus, higher porosity is needed for a loose-sintering technique, its compression yield strength being committed (Table 3). This fact is related to the lack of powder compaction step and low sintering temperatures, without ensuring a good strength of the formed neck (also critical to fatigue and flexural requirements).

Yield strength values are fixed in a range from 150 to 200 MPa meeting the requirements of the cortical bone tissue in Figure 5b, evaluating what occurs with the total porosity, the mean size of the pores (Table 2) and the Young's modulus (Table 3). A complete analysis of the results seen in Figure 5b allows for specifying that only samples processed by a space-holder technique with 40 vol.% could be implemented as substitute of the cortical tissue (bio-mechanical balance between stiffness ~20–25 GPa and mechanical strength, ~150–200 MPa). These specimens present a total porosity of ~37%. Two behaviours of losing mechanical efficiency are observed related respectively to: decreasing compaction pressure by a conventional PM route (reduction of cold welding of titanium powders, weaker necks); and increasing the pore size in a space-holder technique.

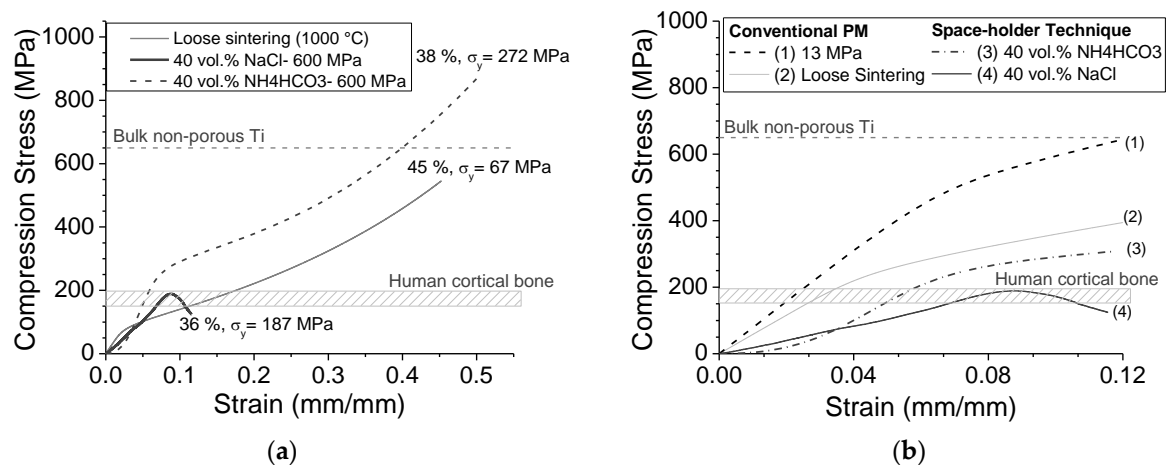


Figure 5. Uniaxial compression tests: (a) Young's modulus closed to the cortical bone is set in ~29 GPa (porosity total range between 37.6–44.8%); (b) yield strength values are fixed in a range (150–200 MPa) meeting the requirements of the cortical tissue. Compression stress vs. Strain curves of specimens manufactured by different PM routes.

The decreasing trend of the relative strength observed in Figure 3a,b undergoes two different performances (see in the slope curves). A proportional and expected loss of the mechanical strength with the reduction of the load section is observed. Then, a part of the strength decrement regarding the pore content, is compensated by the titanium matrix strengthening (see in the lowest slope); this fact occurs in ratio $P_i/P(\text{Arch}) \geq 0.89$ ($P_i = 40\%$) and it is related to the large stress triaxiality originated by more interconnected porosity, in addition to more roughness contour of pores. This strengthening is not representative to the porosity range achieved via conventional PM. The mechanical requirements of cortical bone tissue could be guaranteed in the shaded area in Figure 3b (175–211 MPa). These results are consistent with that proposed by Kubicki [46]: before the mean stress reaches levels close to the yield strength (approx. 33%), in the surrounding area of the notch, it is produced a triaxiality stress state and local plastic strain. As a consequence in ductile material, the yield strength of a notched specimen is higher than the uniaxial one [47]. Therefore, the local plastic strain involves a macroscopic hardening reflected in the yield strength increment of the material [48]. This aspect was observed in Figure 4, where a localized effect of pores was made evident, but a good balance between the mechanical properties was achieved (Table 4), according to the results obtained by the FE model.

5. Conclusions

The assessing of conventional PM and space holder technique reported here allowed for stating some findings about the influence on both microstructural and mechanical properties of porous Ti for bone replacement:

1. Young's modulus of porous Ti samples could be reached close enough to the cortical bone by conventional PM (29 GPa), in the absence of the compaction pressure stage (loose-sintering technique), with a sintering temperature of 1000 °C, and 2 h under high vacuum. However, the mean pore size (~17 μm) and the mechanical strength (~67 MPa) of the porous titanium do not guarantee the mechanical requirements of biomedical applications. Both increments of compaction pressure and sintering temperature improve the quality of the sintering necks, which imply decreasing of the amount and the size of the pores; consequently, the stiffness is increased (≥ 50.5 GPa) and the capability of bone ingrowth.

2. The space-holder method is the more suitable of the two evaluated routes to reach a biomechanical balance (E and σ_y) and biofunctional equilibrium (bone ingrowth), through the control of the processing parameters, the type of space holder, the compaction pressure and the sintering temperature, according to viability, feasibility and implementation costs in the industrial sector, in

addition to the achievement of the desirable balance. The use of NH_4HCO_3 as space holder (40 vol.% and $\sim 200\text{--}300\ \mu\text{m}$ mean particle size distribution) is recommended. The optimal manufacturing parameters proposed are the following ones: firstly, a compaction pressure of 600 MPa, next, in the space-holder elimination stage, $60\ ^\circ\text{C}$ for 10 h plus $110\ ^\circ\text{C}$ for 12 h in vacuum (10^{-2} mbar) and sintering conditions at $1250\ ^\circ\text{C}$, for 2 h and high vacuum (10^{-5} mbar). These parameters ensure the production of porous titanium where the stress-shielding phenomenon is reduced, and suitable mechanical strength and bone ingrowth are achieved.

Author Contributions: All of the authors have contributed to obtaining a high-quality research work. S.L. has been responsible for the experimental results and analysis of data, C.A. and I.M.-M. performed analysis of the results and writing the original draft, S.M. was responsible of finite element analysis, J.A.R.-O. and Y.T. have been responsible for materials and processing techniques selection, funding acquisition and project administration, P.T. was responsible for the fabrication processes and the discussion of the results.

Funding: This work was supported by the Ministry of Economy and Competitiveness of Spain under Grant MAT2015-71284-P, Junta de Andalucía under Grant No. P12-TEP-1401 and the funding provided by the Comisión Nacional de Investigación Científica y Tecnológica (CONICYT) of the Chilean government under the project FONDECYT 11160865.

Acknowledgments: The authors dedicate this paper to the memory of Juan J. Pavón Palacio (University of Antioquia, Colombia) for his valuable contribution in the metal biomaterials field, being a pioneer in this sector and an honourable researcher in the group that has performed this work. The authors wish to thank the laboratory technicians Jesús Pinto and Mari Cruz. Martín, Glenda Hernández and Mauricio Reyes-Valenzuela for carrying out the microstructure characterization and mechanical testing.

Conflicts of Interest: The authors declare no conflict of interest.

References

1. Torres, Y.; Trueba, P.; Pavón, J.; Montealegre, I.; Rodríguez-Ortiz, J. Designing, processing and characterisation of titanium cylinders with graded porosity: An alternative to stress-shielding solutions. *Mater. Des.* **2014**, *63*, 316–324. [[CrossRef](#)]
2. Niinomi, M.; Nakai, M.; Hieda, J. Development of new metallic alloys for biomedical applications. *Acta Biomater.* **2012**, *8*, 3888–3903. [[CrossRef](#)]
3. Xiong, J.; Li, Y.; Wang, X.; Hodgson, P.; Wen, C.E. Mechanical properties and bioactive surface modification via alkali-heat treatment of a porous Ti–18Nb–4Sn alloy for biomedical applications. *Acta Biomater.* **2008**, *4*, 1963–1968. [[CrossRef](#)] [[PubMed](#)]
4. Schmidutz, F.; Agarwal, Y.; Müller, P.; Gueorguiev, B.; Richards, R.; Sprecher, C. Stress-shielding induced bone remodeling in cementless shoulder resurfacing arthroplasty: A finite element analysis and in vivo results. *J. Biomech.* **2014**, *47*, 3509–3516. [[CrossRef](#)] [[PubMed](#)]
5. Herrera, A.; Yáñez, A.; Martel, O.; Afonso, H.; Monopoli, D. Computational study and experimental validation of porous structures fabricated by electron beam melting: A challenge to avoid stress shielding. *Mater. Sci. Eng. C* **2014**, *45*, 89–93. [[CrossRef](#)] [[PubMed](#)]
6. Muñoz, S.; Castillo, S.; Torres, Y. Different models for simulation of mechanical behaviour of porous materials. *J. Mech. Behav. Biomed. Mater.* **2018**, *80*, 88–96. [[CrossRef](#)] [[PubMed](#)]
7. Arabnejad, S.; Johnston, B.; Tanzer, M.; Pasini, D. Fully porous 3D printed titanium femoral stem to reduce stress-shielding following total hip arthroplasty. *J. Orthop. Res.* **2017**, *35*, 1774–1783. [[CrossRef](#)] [[PubMed](#)]
8. Bonfield, W.; Grynblas, M.D.; Tully, A.E. Hydroxyapatite reinforced polyethylene—A mechanically compatible implant material for bone replacement. *Biomaterials* **1981**, *2*, 185–186. [[CrossRef](#)]
9. Geetha, M.; Singh, R.; Asokamani, R.; Gogia, A.K. Ti based biomaterials, the ultimate choice for orthopaedic implants—A review. *Prog. Mater. Sci.* **2009**, *54*, 397–425. [[CrossRef](#)]
10. Aguilar, C.; Guerra, C.; Lascano, S.; Guzman, D.; Rojas, P.A.; Thirumurugan, M.; Bejar, L.; Medina, A. Synthesis and characterization of Ti–Ta–Nb–Mn foams. *Mater. Sci. Eng. C* **2016**, *58*, 420–431. [[CrossRef](#)]
11. Trueba, P. Desarrollo de titanio con porosidad gradiente radial y longitudinal para aplicaciones biomédicas. Ph.D. Thesis, University of Seville, Seville, Spain, 2017.
12. Naebe, M.; Shirvanimoghaddam, K. Functionally graded materials: A review of fabrication and properties. *Appl. Mater. Today* **2016**, *5*, 223–245. [[CrossRef](#)]

13. Singh, S.; Ramakrishna, S.; Singh, R. Material issues in additive manufacturing: A review. *J. Manuf. Process.* **2017**, *25*, 185–200. [[CrossRef](#)]
14. Dewidar, M.M.; Lim, J.K. Properties of solid core and porous surface Ti–6Al–4V implants manufactured by powder metallurgy. *J. Alloys Compd.* **2008**, *454*, 442–446. [[CrossRef](#)]
15. Wenjuan, N.; Chenguang, B.; GuiBao, Q.; Qiang, W. Processing and properties of porous titanium using space holder technique. *Mater. Sci. Eng. A* **2009**, *506*, 148–151.
16. Yavari, S.A.; van der Stok, J.; Chai, Y.C.; Wauthle, R.; Birgani, Z.T.; Habibovic, P.; Mulier, M.; Schrooten, J.; Weinans, H.; Zadpoor, A.A. Bone regeneration performance of surface-treated porous titanium. *Biomaterials* **2014**, *35*, 6172–6181. [[CrossRef](#)] [[PubMed](#)]
17. Torres, Y.; Pavón, J.J.; Nieto, I.; Rodríguez, J.A. Conventional Powder Metallurgy Process and Characterization of Porous Titanium for Biomedical Applications. *Metall. Mater. Trans. B* **2011**, *42*, 891–900. [[CrossRef](#)]
18. Li, Y.; Yang, C.; Zhao, H.; Qu, S.; Li, X.; Li, Y. New Developments of Ti-Based Alloys for Biomedical Applications. *Materials* **2014**, *7*, 1709–1800. [[CrossRef](#)]
19. Torres, Y.; Pavón, J.; Rodríguez, J. Processing and characterization of porous titanium for implants by using NaCl as space holder. *J. Mater. Process. Technol.* **2012**, *212*, 1061–1069. [[CrossRef](#)]
20. Wang, X.; Xu, S.; Zhou, S.; Xu, W.; Leary, M.; Choong, P.; Qian, M.; Brandt, M.; Xie, Y.M. Topological design and additive manufacturing of porous metals for bone scaffolds and orthopaedic implants: A review. *Biomaterials* **2016**, *83*, 127–141. [[CrossRef](#)]
21. Torres, Y.; Lascano, S.; Bris, J.; Pavón, J.; Rodríguez, J.A. Development of porous titanium for biomedical applications: A comparison between loose sintering and space-holder techniques. *Mater. Sci. Eng. C* **2014**, *37*, 148–155. [[CrossRef](#)]
22. Oh, I.H.; Nomura, N.; Masahashi, N.; Hanada, S. Mechanical properties of porous titanium compacts prepared by powder sintering. *Scr. Mater.* **2003**, *49*, 1197–1202. [[CrossRef](#)]
23. Ryan, G.; Pandit, A.; Apatsidis, D.P. Fabrication methods of porous metals for use in orthopaedic applications. *Biomaterials* **2006**, *27*, 2651–2670. [[CrossRef](#)] [[PubMed](#)]
24. Wang, L.; Liu, P.; Wang, L.; Xing, W.; Fan, Y.; Xu, N. Preparation conditions and porosity of porous titanium sintered under positive pressure. *Mater. Manufact. Proce.* **2013**, *28*, 1166–1170. [[CrossRef](#)]
25. Kato, K.; Ochiai, S.; Yamamoto, A.; Daigo, Y.; Honma, K.; Matano, S.; Omori, K. Novel multilayer Ti foam with cortical bone strength and cytocompatibility. *Acta Biomater.* **2013**, *9*, 5802–5809. [[CrossRef](#)] [[PubMed](#)]
26. Torres, Y.; Rodríguez, J.A.; Arias, S.; Echeverry, M.; Robledo, S.; Amigó, V.; Pavón, J.J. Processing, Characterization and biological testing of porous titanium obtained by space-holder technique. *J. Mater. Sci.* **2012**, *47*, 6565–6576. [[CrossRef](#)]
27. Wen, C.E.; Mabuchi, M.; Yamada, Y.; Shimojima, K.; Chino, Y.; Asahina, T. Processing of biocompatible porous Ti and Mg. *Scr. Mater.* **2001**, *45*, 1147–1153. [[CrossRef](#)]
28. Laptev, A.; Bram, M.; Buchkremer, D.; Stover, D. Green strength of powder compacts provided for production of highly porous titanium parts. *Powder Metall.* **2005**, *48*, 358. [[CrossRef](#)]
29. Jia, J.; Siddiq, A.R.; Kennedy, A.R. Porous titanium manufactured by a novel powder tapping method using spherical salt bead space holders: Characterisation and mechanical properties. *J. Mech. Behav. Biomed. Mater.* **2015**, *48*, 229–240. [[CrossRef](#)]
30. Kim, S.W.; Jung, H.-D.; Kang, M.-H.; Kim, H.-E.; Koh, Y.-H.; Estrin, Y. Fabrication of porous titanium scaffold with controlled porous structure and net-shape using magnesium as spacer. *Mater. Sci. Eng. C* **2013**, *33*, 2808–2815. [[CrossRef](#)]
31. Mansourighasri, A.; Muhamad, N.; Sulong, A.B. Processing titanium foams using tapioca starch as a space holder. *J. Mater. Process. Technol.* **2012**, *212*, 83–89. [[CrossRef](#)]
32. Reddy, T.H.; Pal, S.; Kumar, K.C.; Mohan, M.K.; Kokol, V. Finite Element Analysis for Mechanical Response of Magnesium Foams with Regular Structure Obtained by Powder Metallurgy Method. *Procedia Eng.* **2016**, *149*, 425–430. [[CrossRef](#)]
33. Kikuchi, M.; Takahashi, M.; Okuno, O. Elastic Moduli of Cast Ti–Au, Ti–Ag, and Ti–Cu alloys. *Dent. Mater.* **2006**, *22*, 641–646. [[CrossRef](#)]
34. Muñoz, S.; Pavón, J.; Rodríguez-Ortiz, J.; Civantos, A.; Allain, J.; Torres, Y. On the influence of space holder in the development of porous titanium implants: Mechanical, computational and biological evaluation. *Mater. Charact.* **2015**, *108*, 68–78. [[CrossRef](#)]

35. Gibson, L.J.; Ashby, M.F. *Cellular Solids: Structure and Properties*; Cambridge University Press: Cambridge, UK, 1999.
36. Pabst, W.; Gregorová, E. New relation for the porosity dependence of the effective tensile modulus of brittle materials. *J. Mater. Sci.* **2004**, *39*, 3501–3503. [[CrossRef](#)]
37. Knudsen, F. Dependence of mechanical strength of brittle polycrystalline specimens on porosity and grain size. *J. Am. Ceram. Soc.* **1959**, *42*, 376–387. [[CrossRef](#)]
38. Spriggs, R. Expression for effect of porosity on elastic modulus of polycrystalline refractory materials, particularly aluminum oxide. *J. Am. Ceram. Soc.* **1961**, *44*, 628–629. [[CrossRef](#)]
39. Eudier, M. The mechanical properties of sintered low-alloy steels. *Powder Metall.* **1962**, *5*, 278–290. [[CrossRef](#)]
40. Fleck, N.; Smith, R. The mechanical properties of sintered low-alloy steels. *Powder Metall.* **1981**, *3*, 121–125. [[CrossRef](#)]
41. Itälä, A.; Ylanen, H.; Ekholm, C.; Karlsson, K.; Aro, H. Pore diameter of more than 100 micron is not requisite for bone ingrowth in rabbits. *J. Biomed. Mater. Res.* **2001**, *58*, 679–683. [[CrossRef](#)]
42. Stangl, R.; Rinne, B.; Kastl, S.; Hendrich, C. The influence of pore geometry in cp Ti-implants a cell culture investigation. *Eur. Cells Mater.* **2001**, *2*, 1–9. [[CrossRef](#)]
43. Götz, H.E.; Müller, M.; Emmel, A.; Holzwarth, U.; Erben, R.G.; Stangl, R. Effect of surface finish on the osseointegration of laser-treated titanium alloy implants. *Biomaterials* **2004**, *25*, 4057–4064. [[CrossRef](#)] [[PubMed](#)]
44. Lewis, G. Properties of open-cell porous metals and alloys for orthopaedic applications. *J. Mater. Sci. Mater. Med.* **2013**, *24*, 2293–2325. [[CrossRef](#)]
45. Boccaccini, A.R.; Gil, E.; Torres, Y.; Cordero-Arias, L.; Pavón, J.; Rodríguez-Ortiz, J.A.; Borjas, S. Optimization of electrophoretic deposition and characterization of CHITOSAN/45S5 BIOGLASS® composite coatings on porous titanium for biomedical applications. In Proceedings of the International Conference on Electrophoretic Deposition V: Fundamentals and Applications (EPD 2014), Hernstein, Austria, 5–10 October 2014.
46. Kubicki, B. Stress concentration at pores in sintered materials. *Powder Metall.* **1995**, *38*, 295–298. [[CrossRef](#)]
47. Dieter, G. *Mechanical Metallurgy*; McGraw-Hill Book Company: New York, NY, USA, 1988.
48. Straffelini, G. Strain hardening behaviour of powder metallurgy alloys. *Powder Metall.* **2005**, *48*, 189–192. [[CrossRef](#)]



© 2019 by the authors. Licensee MDPI, Basel, Switzerland. This article is an open access article distributed under the terms and conditions of the Creative Commons Attribution (CC BY) license (<http://creativecommons.org/licenses/by/4.0/>).